Naphthalene-1,8-dicarboxylate based zinc coordination polymers: A photophysical study

Pablo Guerrero-García,[a] Javier Cepeda,[b] Mariano Ortega-Muñoz,[c] Jose Angel García,[d] Amparo Navarro,[e] Duane Choquesillo-Lazarte,[f] Sara Rojas,[a] Antonio Rodríguez Diéguez,[a] María Mar Quesada-Moreno,[e]* Iñigo J. Vitórica-Yrezábal[a]*

[a] Departamento de Química Inorgánica, Facultad de Ciencias, Universidad de Granada, 18071, Granada, Spain; vitorica@ugr.es

[b] Departamento de Química Aplicada, Facultad de Química, Universidad del País Vasco/Euskal Herriko Unibertsitatea (UPV/EHU), 20018, Donostia, Spain.

[c] Departamento de Química Orgánica, Facultad de Ciencias, Universidad de Granada, 18071, Granada, Spain;

[d] Departamento de Física, Facultad de Ciencia y Tecnología, Universidad del País Vasco/Euskal Herriko Unibertsitatea (UPV/EHU), 48940, Leioa, Spain.

[e] Departamento de Química Física y Analítica, Facultad de Ciencias Experimentales, Universidad de Jaén, Campus Las Lagunillas, 23071 Jaén, Spain; mqmoreno@ujaen.es
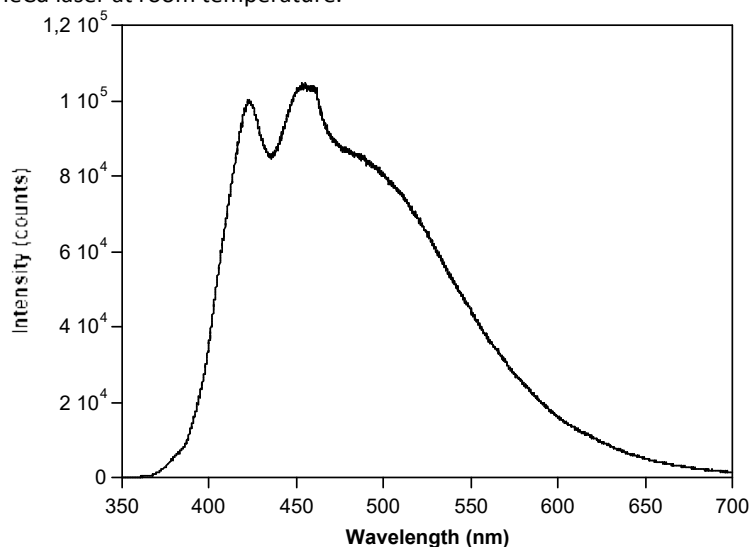
[f.] Laboratorio de Estudios Cristalograficos, IACT, CSIC-Universidad de Granada, Av. De las palmeras 4, Armilla, Granada E-18100, Spain

Supporting Information

S1.   Luminescence properties

The steady-state emission spectrum for the Naphthalene-1,4,5,8-tetracarboxylic acid dianhydride was measured with a HeCd laser at room temperature.


Figure S1. Emission spectrum of Naphthalene-1,4,5,8-tetracarboxylic acid dianhydride (λ_{ex} = 325 nm) at RT.

The spectrum shows two emission maxima (λ_{em} = 422 and 455 nm) in addition to the shoulder peaking at 500 nm. In order to maximize the emission, the excitation spectrum is recorded at the most intense band (λ_{em} = 455 nm), where a relatively narrow maximum on top of a wide band is observed ($\lambda_{ex,max}$ = 405 nm, Figure S2a). Therefore, a second emission spectrum is then recorded with the latter excitation and filtering the emission below 427.5 nm, which is shown in Figure S2b.


(a)   (b)
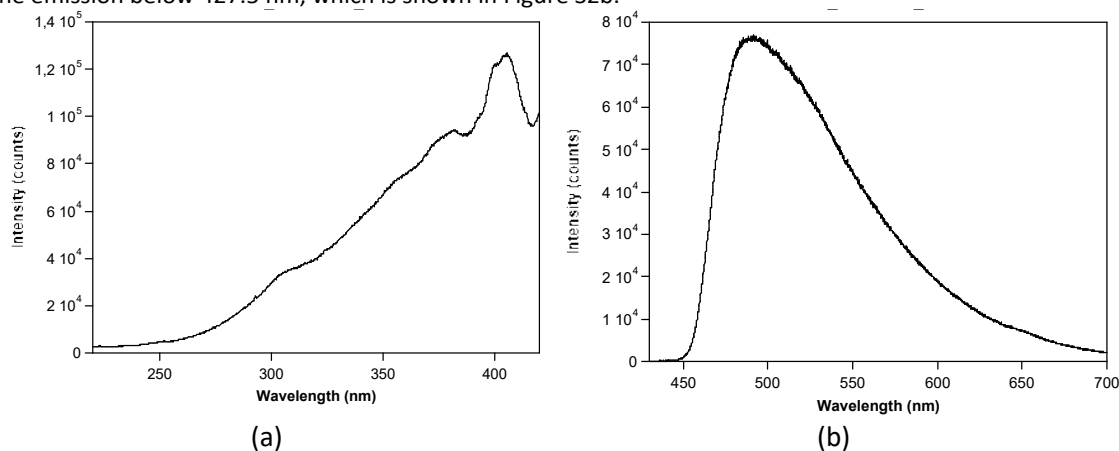
Figure S2. (a) Excitation spectrum of naphthalene-1,4,5,8-tetracarboxylic acid dianhydride recorded at λ_{em} = 455 nm. (b) Emission spectrum with λ_{ex} = 405 nm.

In the following photographs, we observe the emission colour of naphthalene-1,4,5,8-tetracarboxylic acid dianhydride ligand sample as taken in a microscope in which UV illumination can be selected:

2

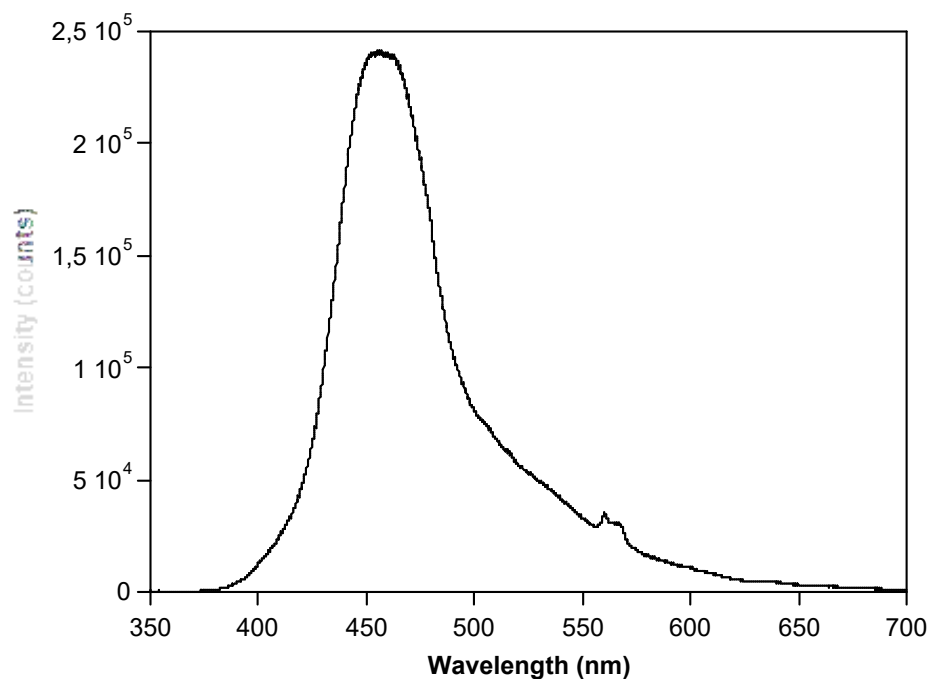(a)   (b)
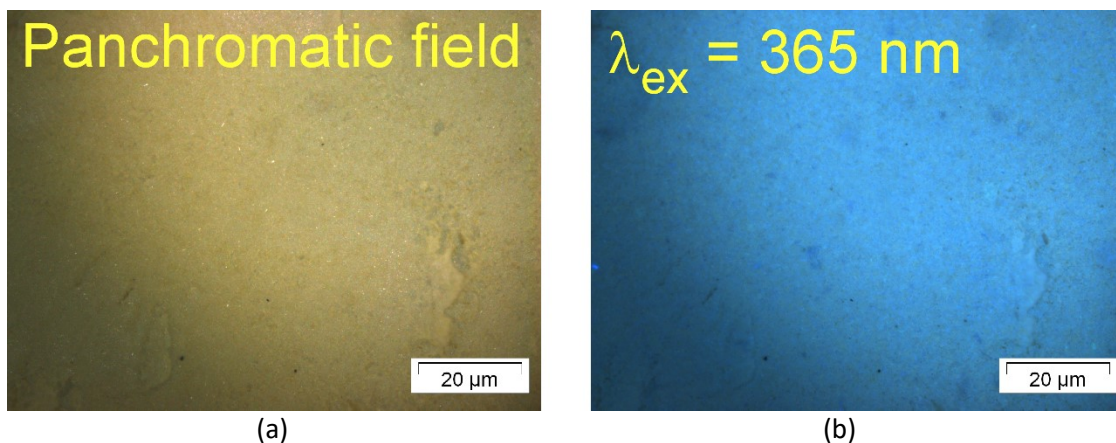
Figure S3. MicroPL photographs of naphthalene-1,4,5,8-tetracarboxylic acid dianhydride sample taken on a microscope illuminated with (a) panchromatic field and (b) UV light.

Finally, a decay curve of naphthalene-1,4,5,8-tetracarboxylic acid dianhydride ligand sample was measured to estimate the emission lifetime of the most intense emission wavelength. The signal had to be deconvoluted with respect to the pulse in order to reliably estimate the lifetime (Figure S4). The fitting gives a mean lifetime of 5.6(1) ns.
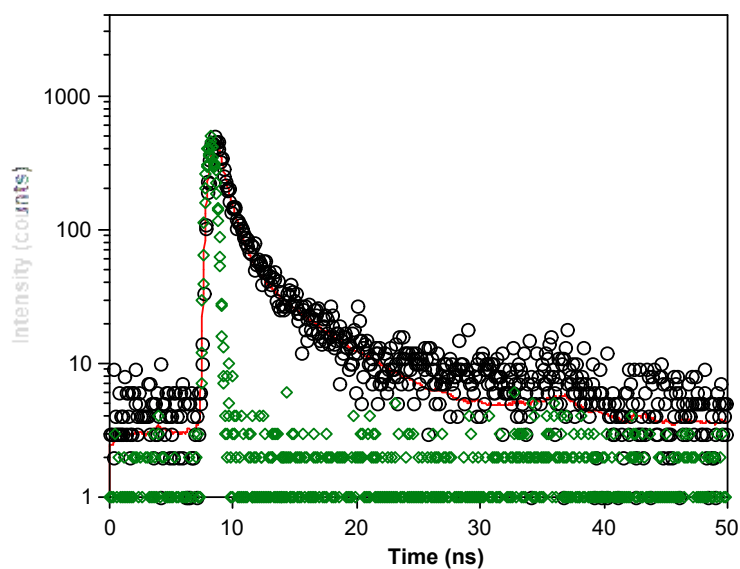

Figure S4. Decay curve measured (in black) with a laser diode (λ_{ex} = 370 nm, λ_{em} = 455 nm) at RT. Colour code: green dots correspond to the instrument response file from the pulsed laser diode LDH-P-C-375 (λ = 375 nm) from PicoQuant as excitation source; black dots corresponds to the decay curve measured and the red line to the fitting of the decay curve with the deconvolution of the pulsed laser signal.

The emission spectrum of H_3L ligand is measured with the same experimental setup used for naphthalene-1,4,5,8-tetracarboxylic acid dianhydride, and is shown in Figure S5.

Figure S5. Emission spectrum of H_3L at RT (λ_{ex} = 325 nm).

The spectrum shows a unique band peaking at λ_{em} = 460 nm. The excitation spectrum was therefore conducted at that wavelength (Figure S6), and shows no observable maximum below the emission line that starts at 400 nm. These results seem to indicate that the ligand possesses a very small Stokes shift.
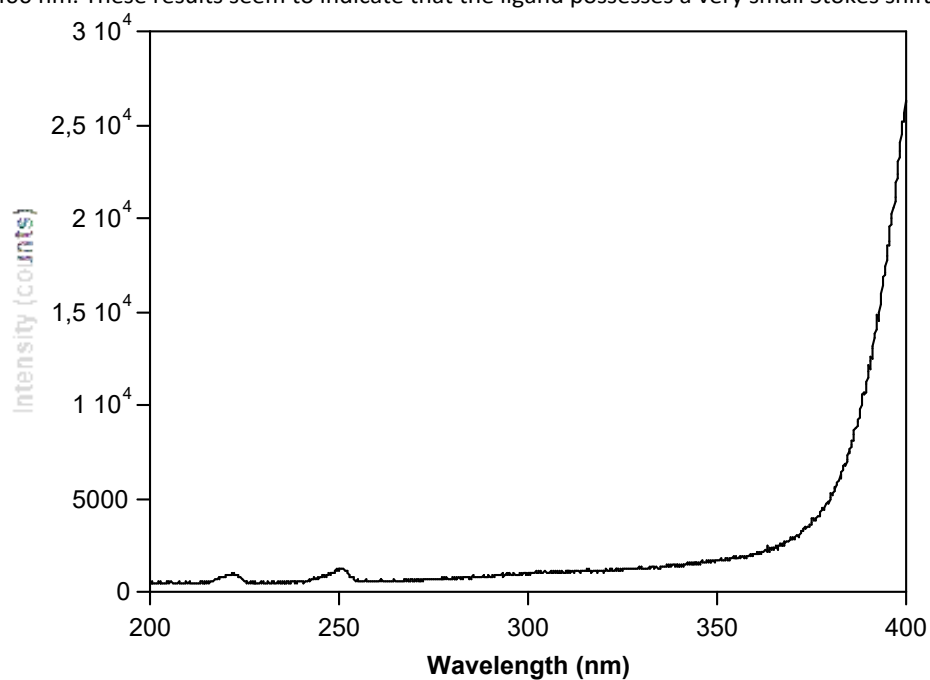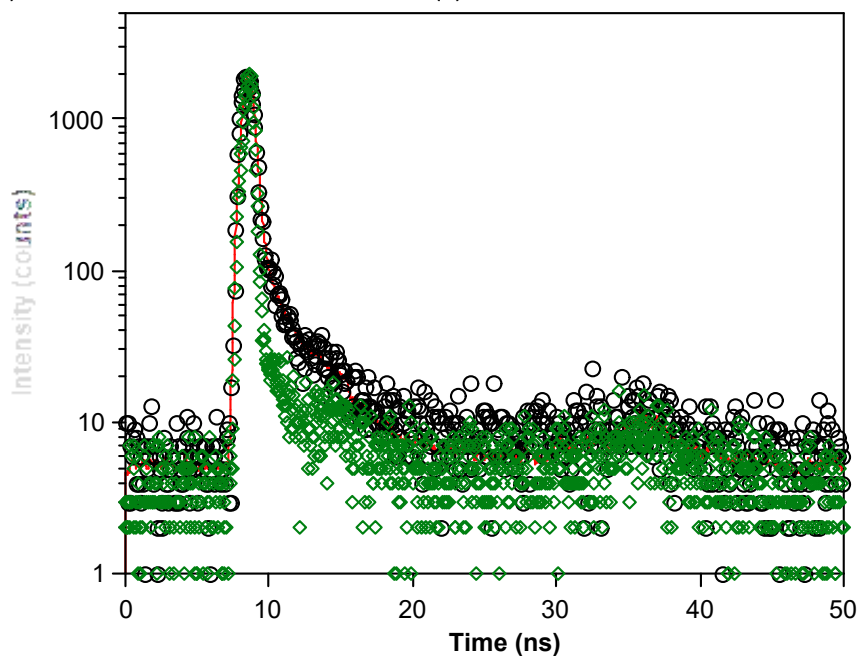

Figure S6. Excitation spectrum of H_3L recorded at λ_{em} = 460 nm and RT.
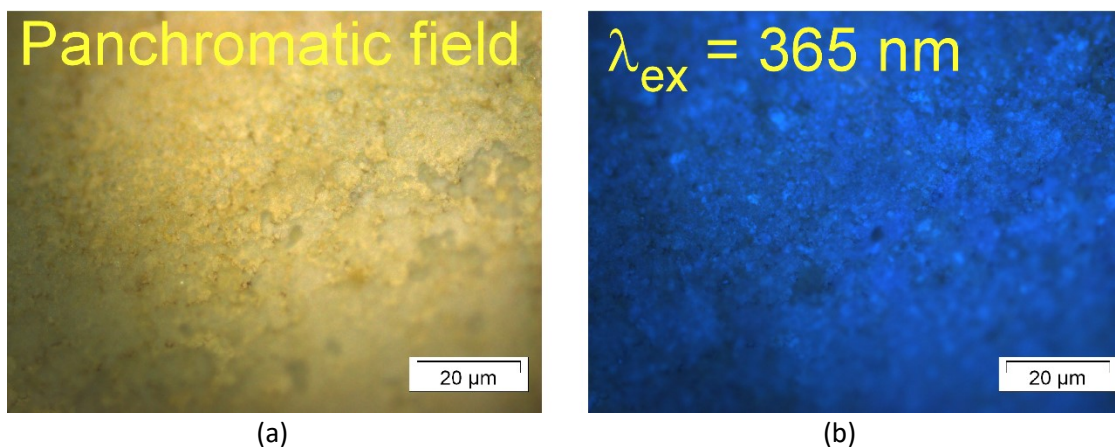
Figure S7. MicroPL photographs of H_3L sample taken on a microscope illuminated with (a) panchromatic field and (b) UV light.

The emission decay lifetime of H_3L was measured with the same previous setup (λ_{ex} = 370 nm and λ_{em} = 460 nm, Figure S8). The estimated mean lifetime is of 1.00(3) ns.


Figure S8. RT emission decay curve (black dots) and pulse reference curve (green dots) showing the fitting with the deconvolution (red line) (λ_{ex} = 370 nm and λ_{em} = 458 nm). Colour code as Figure S4.

The excitation spectra were recorded for the two emission maxima (main band and shoulder) for compound **1**, in which a weak but well defined band is observed for the spectrum recorded at the longest wavelenght (λ_{em} = 530 nm, see Figure S9).

(a)   (b)
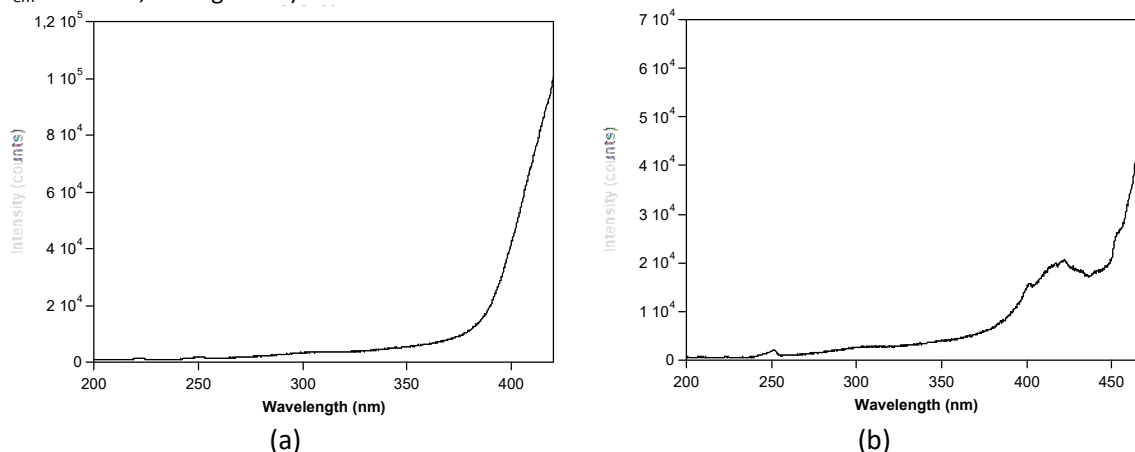
Figure S9. Excitation spectra of **1** recorded for (a) λ_{em} = 460 nm and (b) λ_{em} = 530 nm.

Focusing on the excitation maximum (λ_{ex} = 420 nm, shown in Fig. S9b), the compound presents an emission consistent with the laser excitation (Figure S10).
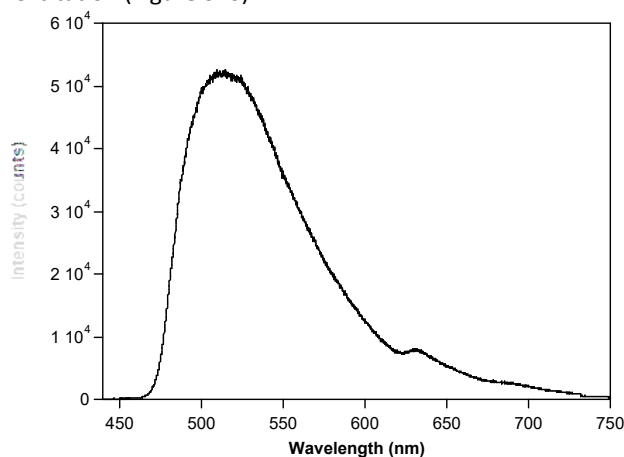

Figure S10. Emission spectrum recorded with λ_{ex} = 420 nm a RT.

At last, the emission lifetimes have been estimated from the decay curves acquired on both emission maxima (λ_{em} = 460 nm y 525 nm), with the aim to corroborate that both bands possess a similar emission to that described for the H_3L ligand (Figure S11). The mean lifetimes obtained are 1.44(1) and 3.3(1) ns respectively for λ_{em} = 460 nm y 525 nm.


(a)   (b)
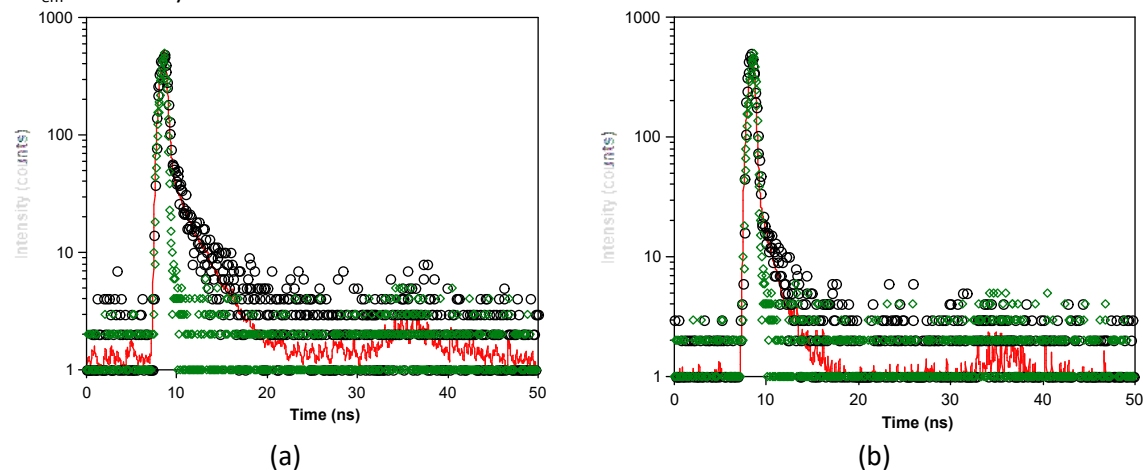
Figure S11. Decay curves for **1** recorded with λ_{ex} = 370 nm for (a) λ_{em} = 460 nm and (b) λ_{em} = 525 nm at RT. Colour code as Figure S4.

6

The excitation spectra of compound **2** acquired at the most intense wavelengths (λ_{em} = 430 nm and λ_{em} = 535 nm) do not show any significant band before the increase corresponding to the emission band (Figure S12).

(a)   (b)
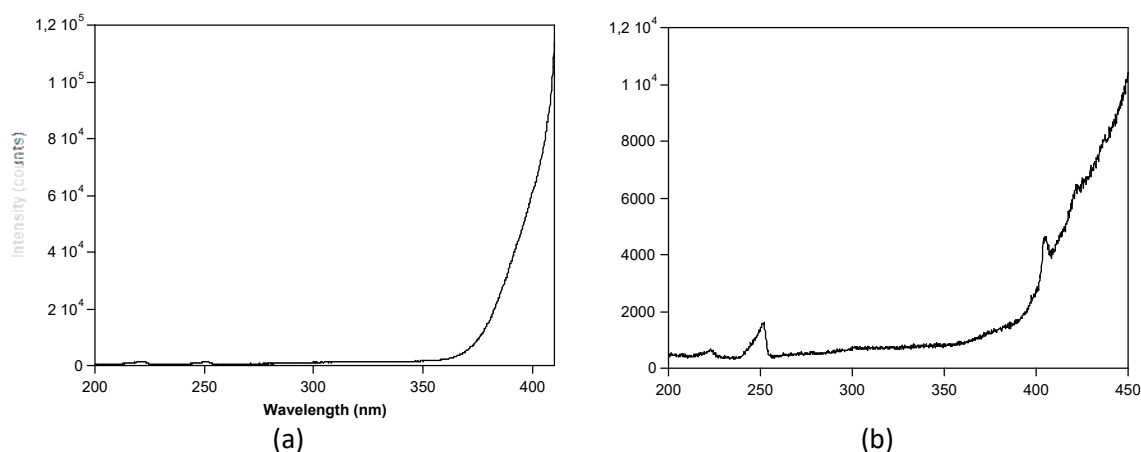
Figure S12. Excitation spectra for compound **2** at (a) λ_{em} = 430 nm and (b) λ_{em} = 535 nm.

The emission lifetimes have been also measured for this sample above both bands (λ_{em} = 430 nm and 535 nm, see Figure S13). From the deconvolution of the weak signals from the pulse reference we obtain mean lifetimes of 0.89(3) ns and 2.79(2) ns.


(a)   (b)
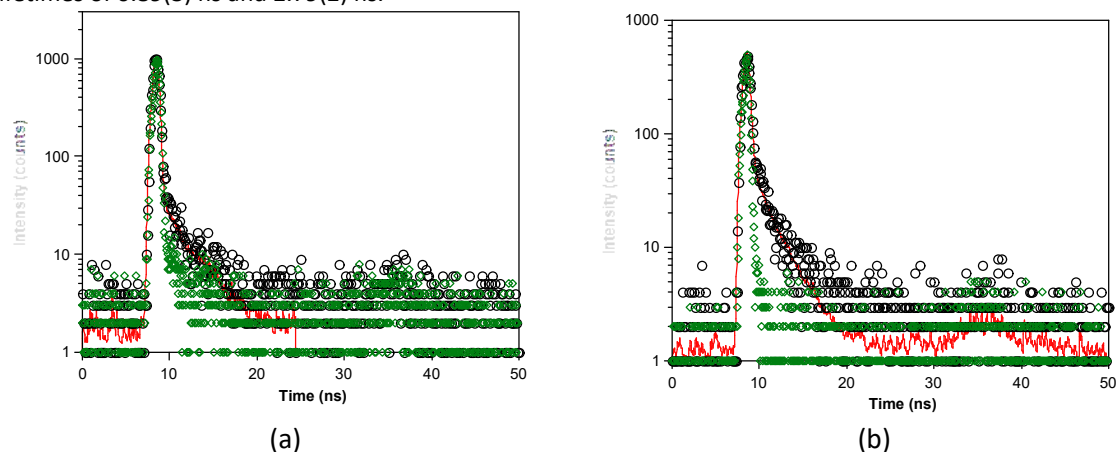
Figure S13. Emission decay curves for **2** recorded with λ_{ex} = 370 nm under (a) λ_{em} = 430 nm and (b) λ_{em} = 530 nm at RT. Colour code as Figure S4

Compound **3** presents a main band that is somewhat structured (λ_{em} = 430 and 450 nm). The excitation spectra recorded over both wavelengths clearly shows the same pattern, characterized for a main excitation band with the maximum at 380 nm (Figure S14).

(b)
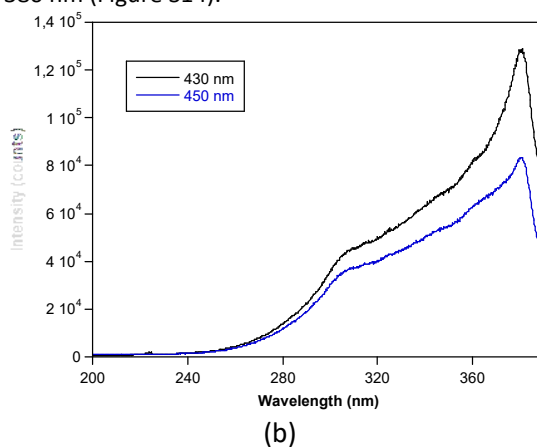
Figure S14. Excitation spectra of **3** for the two main contributions of the emission band (λ_{em} = 430 and 450 nm).

Finally, we measured the decay curves for both main contributions and found quite different lifetimes of 3.25(1) and 0.47(3) ns respectively for λ_{em} = 430 nm y 450 nm (Figure S15).

(a)   (b)
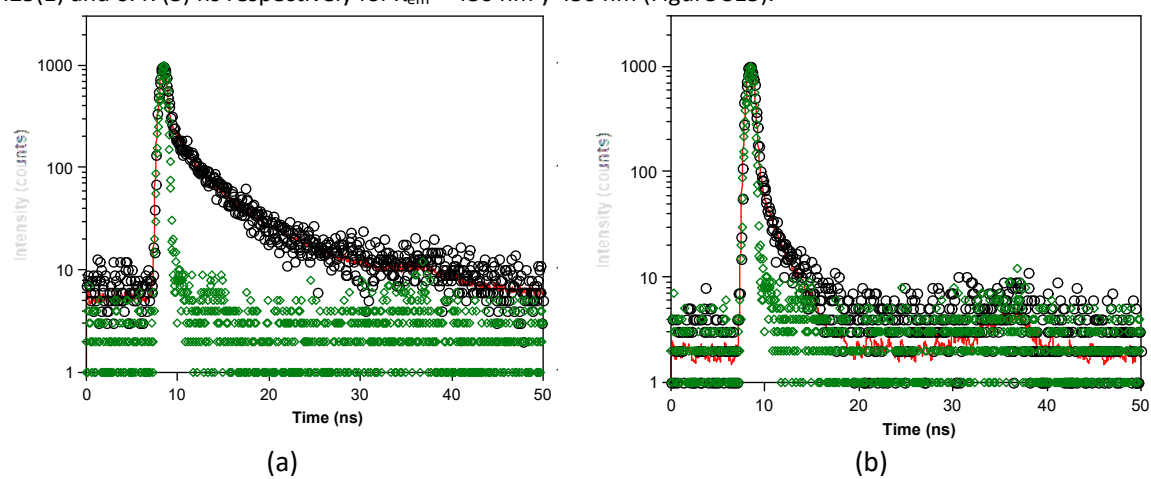
Figure S15. Decay curves of compound **3** recorded with λ_{ex} = 370 nm under (a) λ_{em} = 430 nm and (b) λ_{em} = 450 nm at RT. Colour code as Figure S4

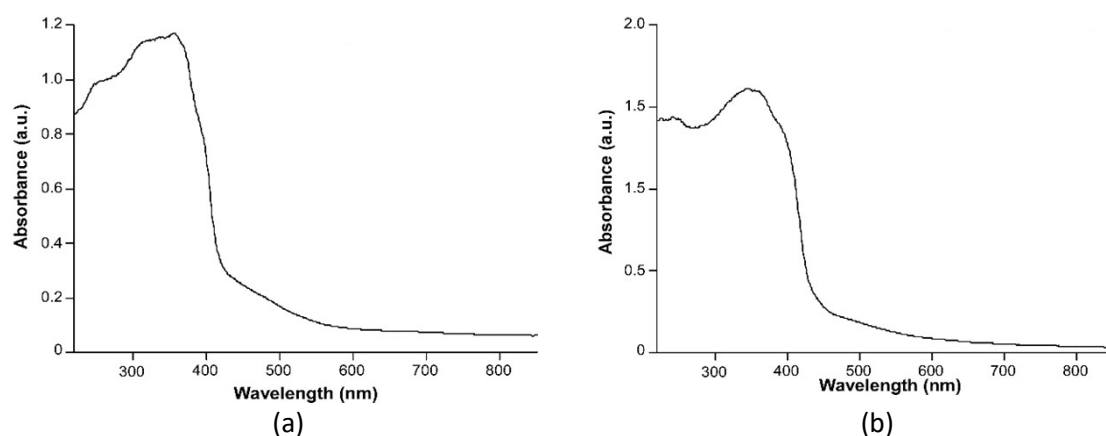## S2.   Diffuse reflectance measurements

(a)

(b)

Figure S16. Diffuse reflectance absorption spectra of free-ligand samples at RT: (a) Naphthalene-1,4,5,8-tetracarboxylic acid dianhydride and (b) H$_3$L.

(a)

(b)

(c)

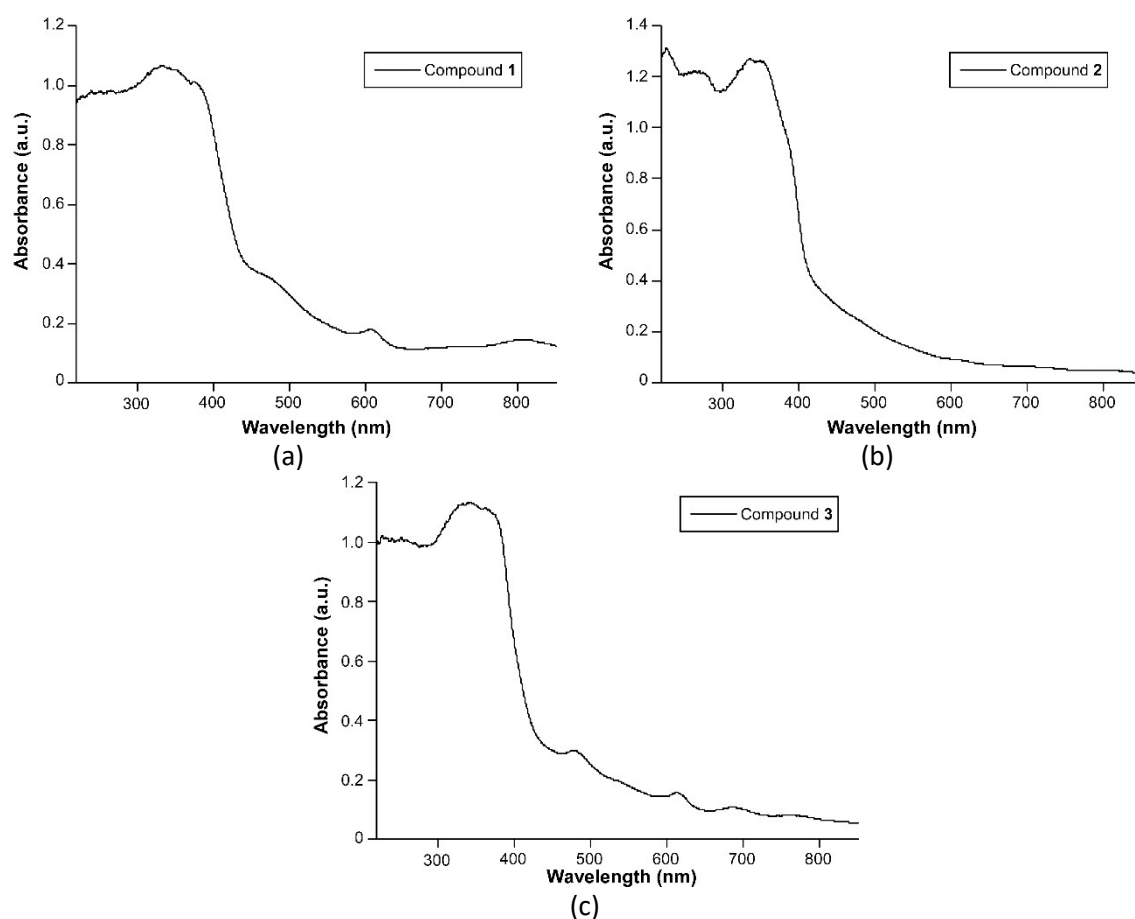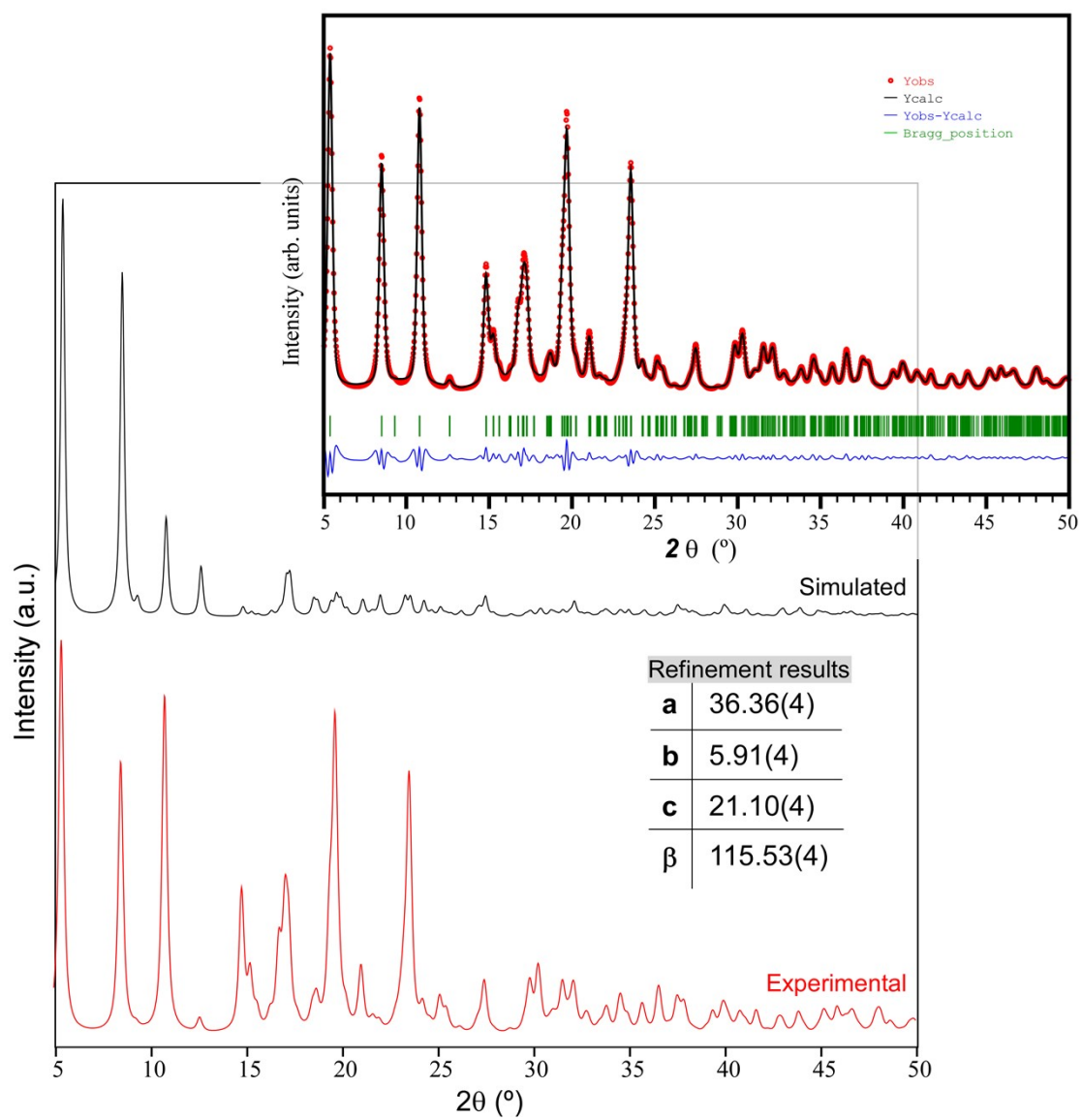**Figure S17.** Diffuse reflectance absorption spectra of all compounds: (a) **1**, (b) **2** and (c) **3**.

S3. Powder X-ray diffraction

Figure S18. Comparison between the experimental and simulated diffractograms of compound **1** together with the pattern-matching analysis and unit cell values.
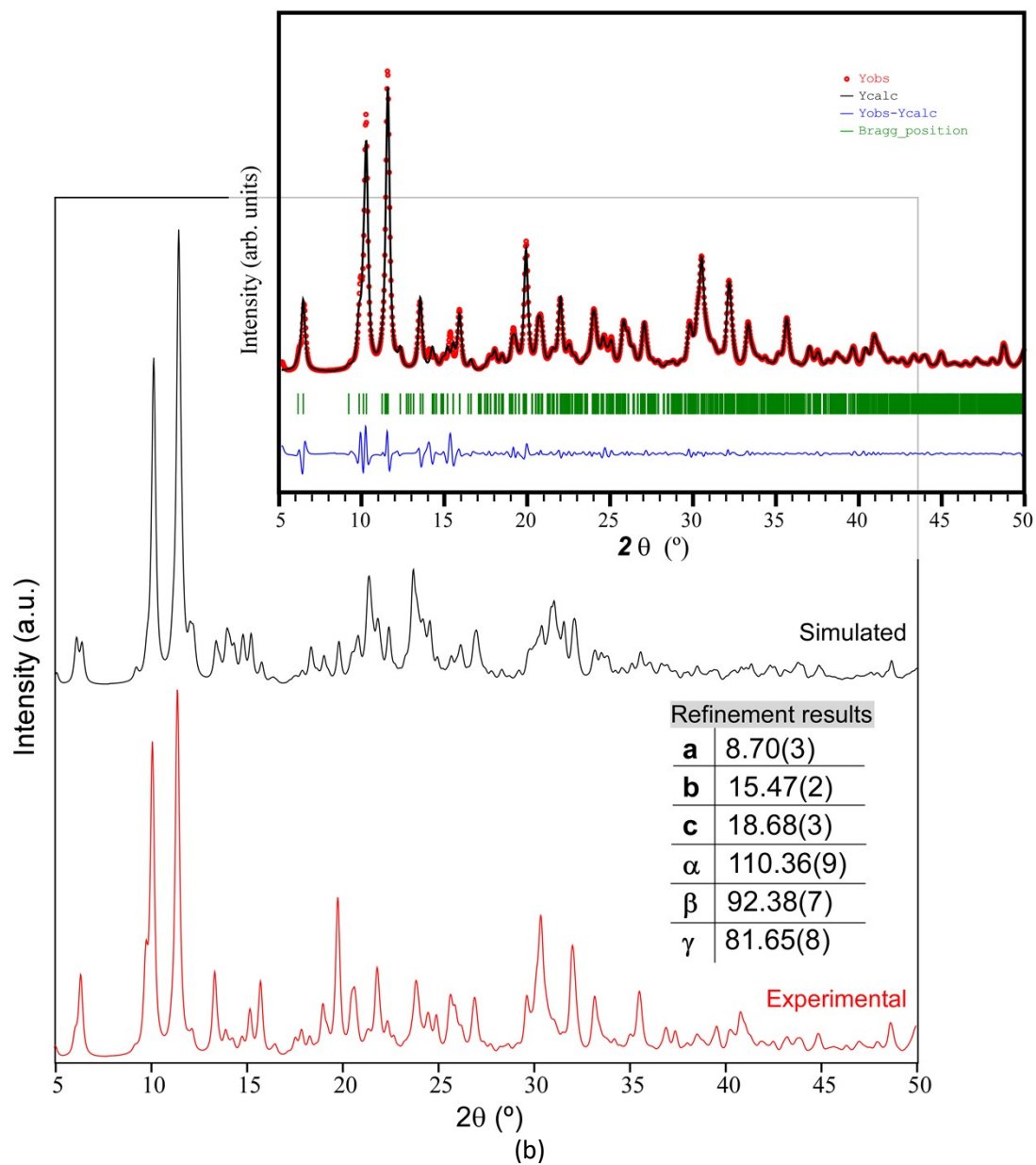
Figure S19. Comparison between the experimental and simulated diffractograms of compound **2** together with the pattern-matching analysis and refined unit cell values.

Refinement results

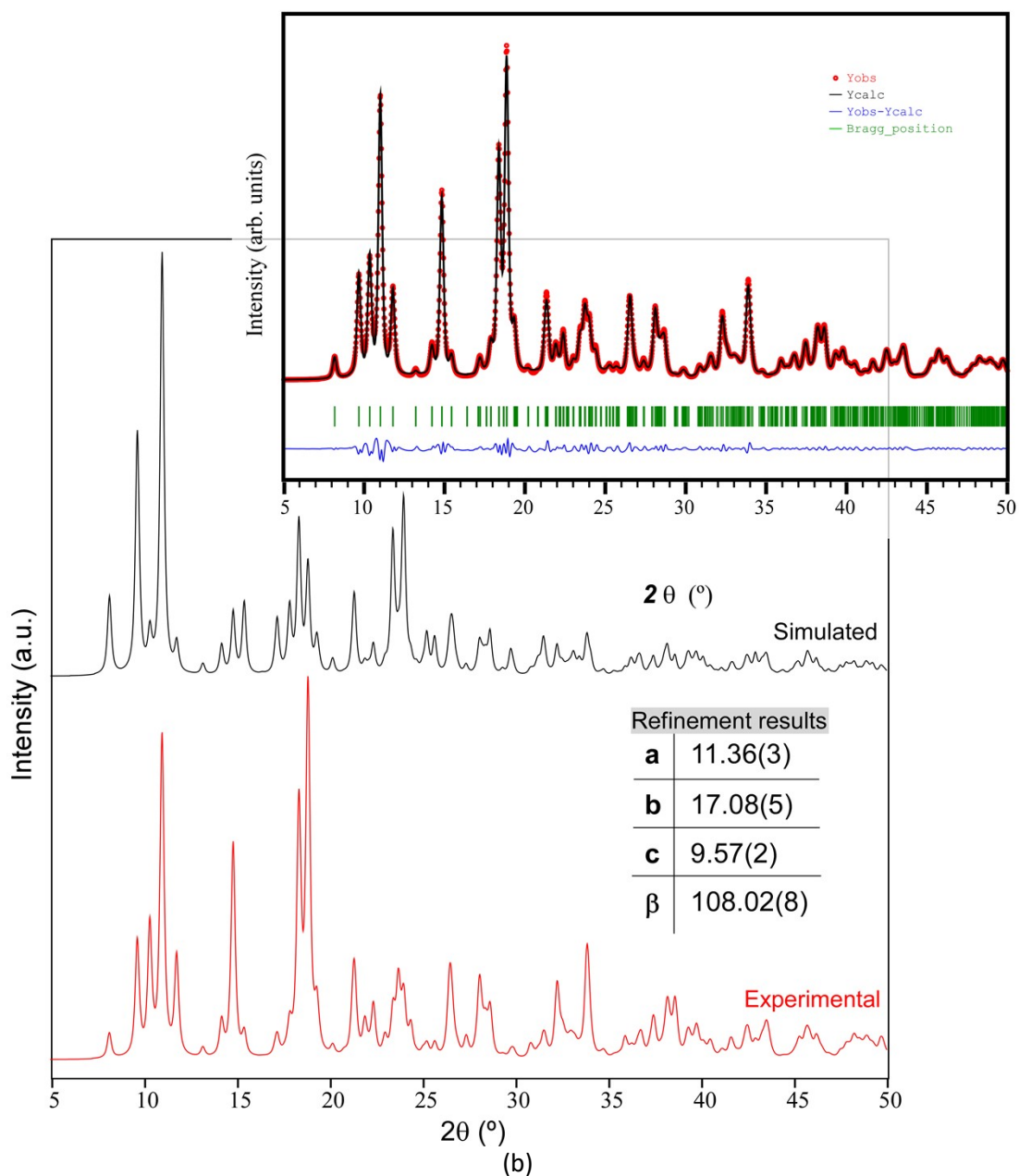|	
a	11.36(3)
b	17.08(5)
c	9.57(2)
β	108.02(8)

Figure S20. Comparison between the experimental and simulated diffractograms of compound **3** together with the pattern-matching analysis and refined unit cell values.

S4. DFT calculations

Table S1. Experimental absorption wavelength (λ_{ab}^{exp}), theoretical vertical electronic transitions ($\lambda_{vert-ab}^{calc}$), oscillator strength (f) and the main molecular orbital contributions (≥10%) calculated at the CAM-B3LYP-D3/6-31G**+LANL2DZ level of theory in gas phase for compounds **1**-**3**. Selected molecular orbitals are represented in Figure S22.

Comp	λ_{ab}^{exp}	$\lambda_{vert-ab}^{calc}$	Transition	f	Contribution
1	606 (2.05)	621 (2.00)	S$_0$→S$_1$	0.0031	HOMO→LUMO (14%); HOMO-2→LUMO+3 (15%); HOMO →LUMO+3 (42%)
		563 (2.20)	S$_0$→S$_6$	0.0714	HOMO-3→LUMO+1 (36%), HOMO-3→LUMO+1 (15%)
		476 (2.60)	S$_0$→S$_9$	0.0012	HOMO-6→LUMO+3 (50%)
	373 (3.32)(sh),	397 (3.12)	S$_0$→S$_{13}$	0.0020	HOMO-5→LUMO (22%), 338→343 (20%), 340→343 (40%)
	333 (3.72)	**333 (3.72)**	**S$_0$→S$_{39}$**	**0.5521**	**HOMO-12→LUMO+1(10%); HOMO-14→LUMO+1(10%)**
		316 (3.93)	S$_0$→S$_{51}$	0.1543	HOMO-13→LUMO+6 (11%); HOMO-3→LUMO+5(10%)
		286 (4.33)	S$_0$→S$_{72}$	0.1288	HOMO-22→LUMO+1(10%)
2		668 (1.86)	S$_0$→S$_1$	0.0000	HOMO→LUMO (99%)
		508 (2.44)	S$_0$→S$_7$	0.0001	HOMO-6→LUMO (94%)
		440 (2.82)	S$_0$→S$_{15}$	0.0079	HOMO-1→LUMO+4 (59%); HOMO→LUMO+4 (22%)
	336 (3.69)	**332 (3.73)**	**S$_0$→S$_{36}$**	**0.0978**	**HOMO-14→LUMO+1(18%); HOMO-13→LUMO+1(58%)**
		326 (3.80)	**S$_0$→S$_{39}$**	**0.0944**	**HOMO-12→LUMO+4 (82%)**
		316 (3.92)	S$_0$→S$_{42}$	0.0402	HOMO-18→LUMO (25%)
		316 (3.93)	S$_0$→S$_{43}$	0.0717	HOMO-12→LUMO+2 (23%); HOMO-9→LUMO+2 (19%); HOMO-7→LUMO+2 (22)
		309 (4.01)	**S$_0$→S$_{46}$**	**0.2107**	**HOMO-14→LUMO+2 (26%); HOMO-13→LUMO+2 (26%); HOMO-7→LUMO+2 (26%)**
3		873 (1.42)	S$_0$→S$_1$	0.0000	HOMO→LUMO (99%)
	613 (2.00)	530 (2.34)	S$_0$→S$_{11}$	0.1886	HOMO-13→LUMO (75%)
	479 (2.59)	450 (2.76)	S$_0$→S$_{18}$	0.0151	HOMO-31→LUMO (15%); HOMO-10→LUMO (36); HOMO-9→LUMO (22%)
		424 (2.92)	S$_0$→S$_{20}$	0.0219	HOMO-31→LUMO (21%); HOMO-12→LUMO (54%)
		370 (3.35)	S$_0$→S$_{33}$	0.0876	HOMO-14→LUMO+2 (20%); HOMO-11→LUMO+2 (68%)
	340 (3.64)	**346 (3.59)**	**S$_0$→S$_{47}$**	**0.3046**	**HOMO-14→LUMO+2(24%); HOMO-10→LUMO+4(17%); HOMO-9→LUMO+4(18%)**
		318 (3.90)	**S$_0$→S$_{62}$**	**0.2037**	**HOMO-13→LUMO+1 (43%)**

Table S2. Experimental excitation ($\lambda_{ex,max}^{exp}$) and emission ($\lambda_{emis,max}^{exp}$), and theoretical emission ($\lambda_{vert-emis}^{calc}$) in nm(eV) calculated at the CAM-B3LYP-D3/6-31G**+ LANL2DZ level of theory in the gas phase for compounds **1**-**3**.

Compound	$\lambda_{ex,max}^{exp}$	$\lambda_{emis,max}^{exp}$	τ (ns)	QY (%)	$\lambda_{vert-emis}^{calc}$	Transition
1	420 (2.95)	465 (2.67)	1.44	2.7(7)	437 (2.84)	$S_{13} \rightarrow S_0$
		525 (2.36)	3.32		511 (2.43)	$S_9 \rightarrow S_0$
2	423 (2.93)	430 (2.88)	0.89	0.7(3)	450 (2.75)	$S_{15} \rightarrow S_0$
		535 (2.32)	2.79		539 (2.30)	$S_7 \rightarrow S_0$
3	380 (3.26)	430 (2.88)	3.25	2.1(6)	426 (2.91)	$S_{20} \rightarrow S_0$
		450 (2.76)	0.47		452 (2.74)	$S_{18} \rightarrow S_0$

Compound 1

Compound 2

Compound 3
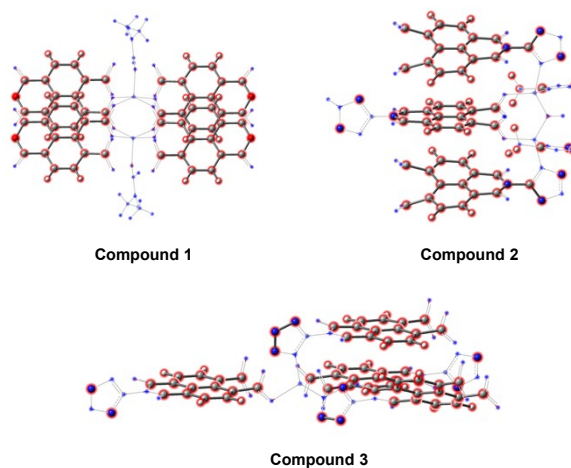
Figure S21. The molecular geometry of the active part of the fragment (in red) optimized at the CAM-B3LYP-D3/6-31G**+LANL2DZ level of theory. The cartesian coordinates of the surrounding molecules (in blue) are frozen.
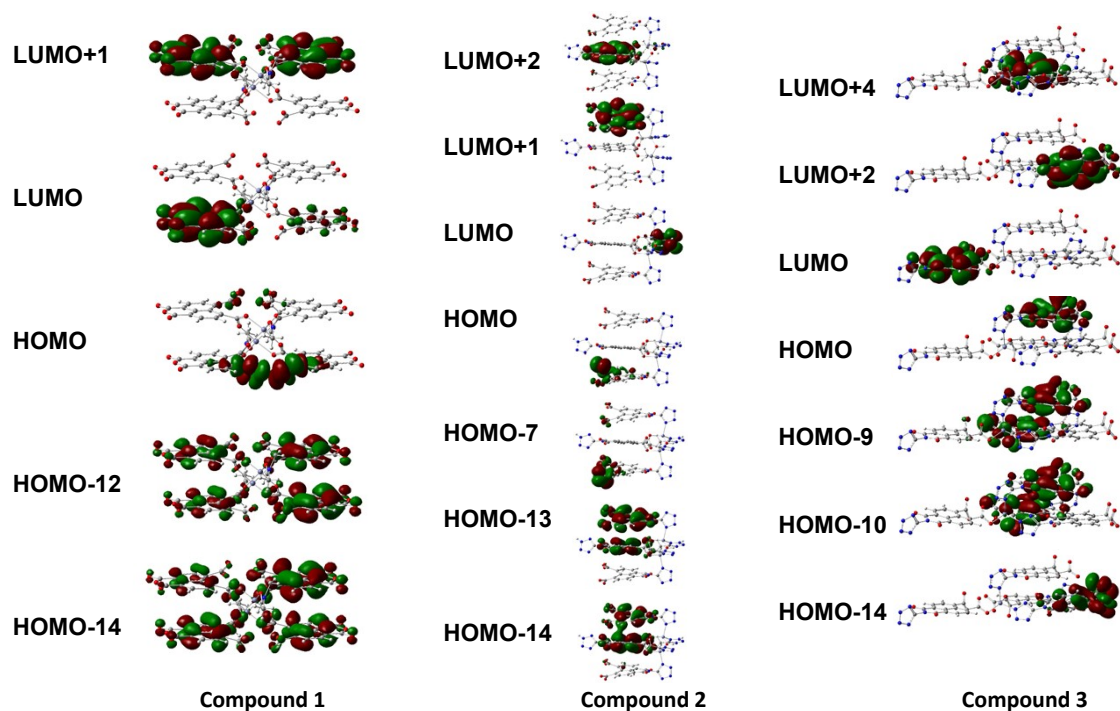
Figure S22. Molecular orbital representation (isocontour plots 0.02 a.u.) of the molecular orbitals involved in the main electronic vertical transitions calculated at the CAM-B3LYP-D3/6-31G**+LANL2DZ level of theory in gas phase for compounds **1**, **2** and **3**.
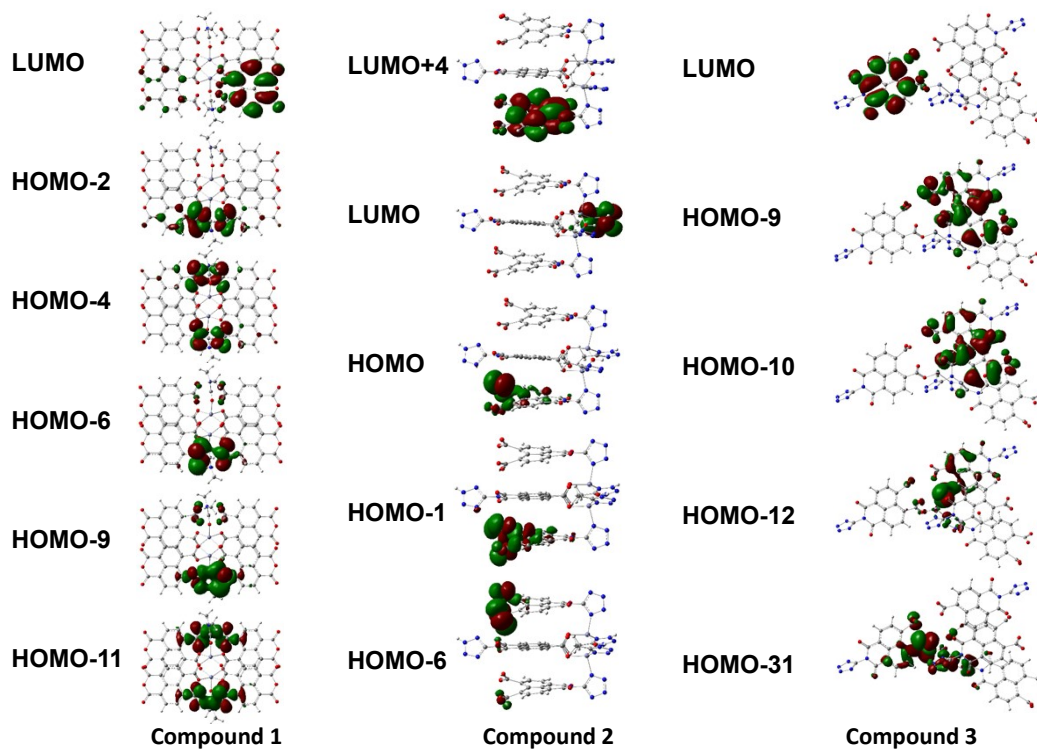
Figure S23. Molecular orbital representation (isocontour plots 0.02 a.u.) of the molecular orbitals involved in the main electronic relaxation calculated at the CAM-B3LYP-D3/6-31G**+LANL2DZ level of theory in gas phase for compounds **1**, **2** and **3**.

S5. Crystallography

Single crystal X-ray diffraction data were collected at 100 K on a Bruker D8 Venture and Bruker APEX-II diffractometers using Cu Kα (λ = 1.5418 Å) and Mo Kα (λ = 0.71073 Å) equipped with a PHOTON 3 and APEX II detectors, and an Oxford cryosystem. Data were collected and processed using APEX II and APEX III software. Adsorption correction was applied using SADABS software by empirical methods measuring symmetry equivalent reflections at different azmuthial angles. All structures were solved using the SHELXT program and refined using least squares refinement methods on all F^2 values as implemented within SHELXL.[S1-S2] Both SHELXT and SHELXL were operated through the Olex2 (v1.5) interface.[S3] All atoms were refined anisotropic and atomic displacement parameters were refined with suitable restraints or constraints applied to keep them physically reasonable. Hydrogen atoms were placed in calculated positions and refined with idealised geometries and assigned fixed occupancies and isotropic displacement parameters. DMF molecules were found disordered and modelled over two sites in the inter-polymer space in compound **1**. CCDC 2312265-2312267 contain the supplementary crystallographic data for this paper. These data can be obtained free of charge via www.ccdc.cam.ac.uk/data_request/cif, or by emailing data_request@ccdc.cam.ac.uk, or by contacting The Cambridge Crystallographic Data Centre, 12 Union Road, Cambridge, CB2 1EZ, UK; fax: +44 1223 336033

Table S3. Crystallographic parameters

Identification code	**1**	**2**	**3**
Empirical formula	$C_{20}H_{18}N_2O_9Zn$	$C_{18}H_{19}N_{11}O_9Zn_2$	$C_{17}H_{12}N_6O_6Zn$
Formula weight	495.73	664.18	461.70
Temperature/K	100(2)	100.00	100(2)
Crystal system	monoclinic	triclinic	monoclinic
Space group	C2/c	P-1	P2$_1$/c
a/Å	36.361(4)	8.7045(3)	11.3657(7)
b/Å	5.9049(6)	15.5177(5)	17.0847(14)
c/Å	21.101(2)	18.7098(6)	9.5700(8)
α/°	90	110.770(2)	90
β/°	115.569(3)	92.200(2)	107.990(2)
γ/°	90	91.272(2)	90
Volume/Å^3	4086.8(7)	2359.49(14)	1767.4(2)
Z	8	4	4
ρ$_{calc}$g/cm^3	1.611	1.870	1.735
μ/mm^{-1}	2.189	3.196	1.443
F(000)	2032.0	1344.0	936.0
Crystal size/mm^3	0.12 × 0.1 × 0.1	0.06 × 0.02 × 0.02	0.1 × 0.1 × 0.09
Radiation	CuKα (λ = 1.54178)	CuKα (λ = 1.54178)	MoKα (λ = 0.71073)
2Θ range for data collection/°	9.292 to 133.626	5.058 to 133.188	4.458 to 55.014
Index ranges	-42 ≤ h ≤ 42, -7 ≤ k ≤ 7, -22 ≤ l ≤ 25	-10 ≤ h ≤ 10, -18 ≤ k ≤ 18, -22 ≤ l ≤ 22	-12 ≤ h ≤ 14, -22 ≤ k ≤ 22, -12 ≤ l ≤ 12
Reflections collected	16962	43035	32089
Independent reflections	3559 [R$_{int}$ = 0.0372, R$_{sigma}$ = 0.0310]	8292 [R$_{int}$ = 0.2427, R$_{sigma}$ = 0.1800]	4058 [R$_{int}$ = 0.0599, R$_{sigma}$ = 0.0356]
Data/restraints/parameters	3559/382/357	8292/9/732	4058/0/301
Goodness-of-fit on F^2	1.072	0.998	1.059
Final R indexes [I>=2σ (I)]	R$_1$ = 0.0413, wR$_2$ = 0.1254	R$_1$ = 0.1002, wR$_2$ = 0.2424	R$_1$ = 0.0303, wR$_2$ = 0.0725
Final R indexes [all data]	R$_1$ = 0.0426, wR$_2$ = 0.1272	R$_1$ = 0.1970, wR$_2$ = 0.3087	R$_1$ = 0.0389, wR$_2$ = 0.0785
Largest diff. peak/hole / e Å^{-3}	0.79/-0.57	1.85/-0.89	0.54/-0.24

S6. Nuclear magnetic resonance
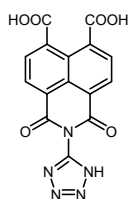
1,3-dioxo-2-(1H-tetrazol-5-yl)-2,3-dihydro-1H-benzo[de]isoquinoline-6,7-dicarboxylic   acid (**C$_{14}$H$_7$N$_5$O$_6$**) (H$_3$L) 1H NMR (400 MHz, DMSO-d6) δ 13.69 (s, 2H), 8.57 (d, J = 7.5 Hz, 2H), 8.21 (d, J = 7.7 Hz, 2H). 13C NMR (101 MHz, DMSO) δ 168.20, 160.10, 137.42, 131.61, 130.74, 129.35, 125.42, 121.91
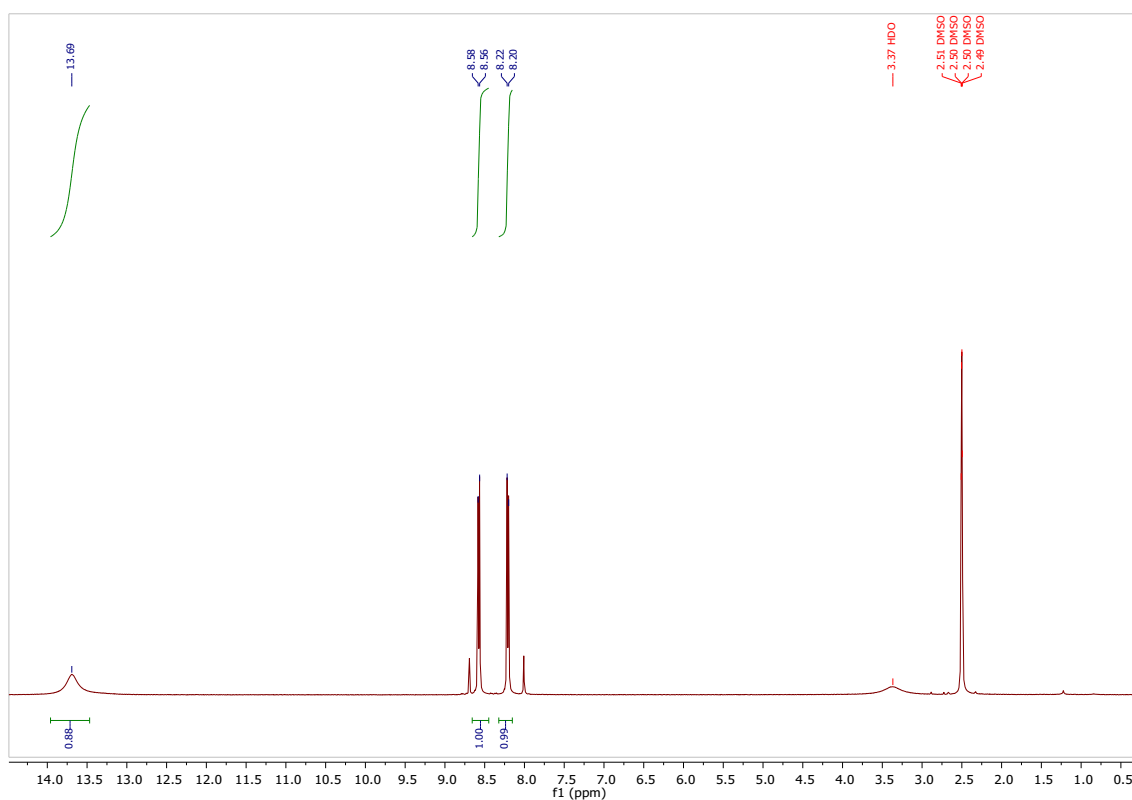
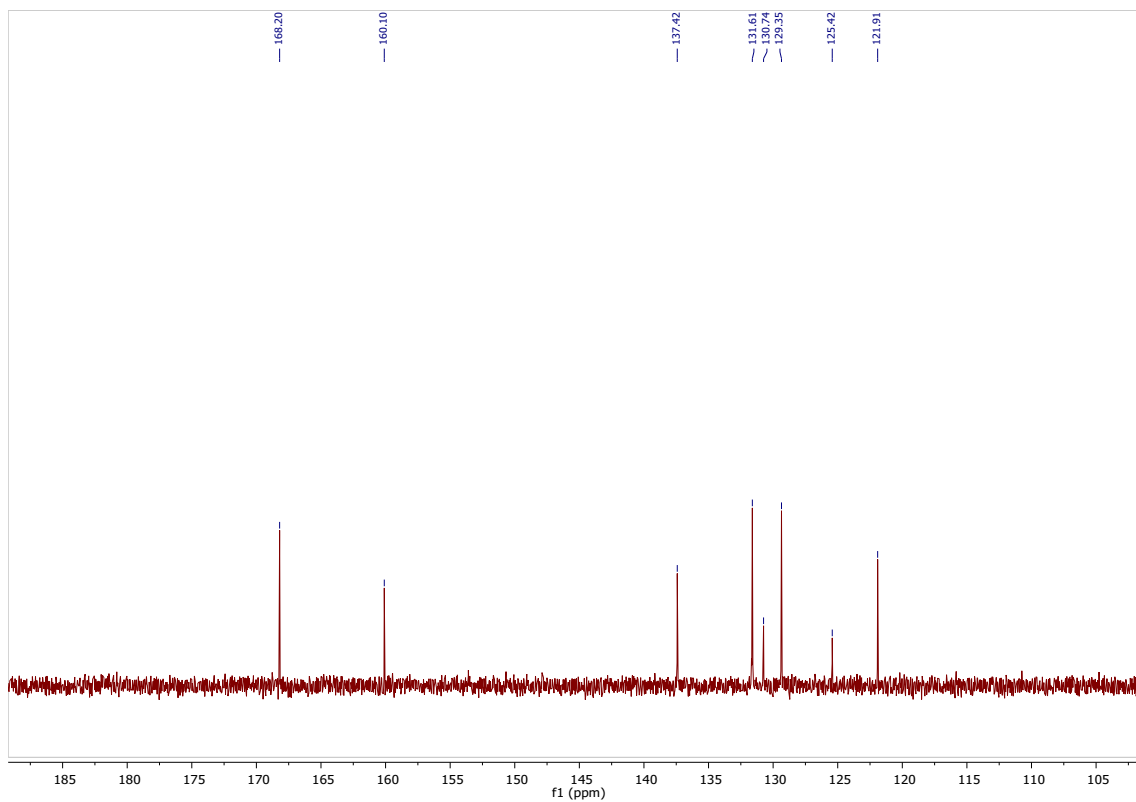**Figure S24.** ^{1}H NMR (400 MHz, DMSO-d_6) δ 13.69 (s, 2H), 8.57 (d, J = 7.5 Hz, 2H), 8.21 (d, J = 7.7 Hz, 2H).

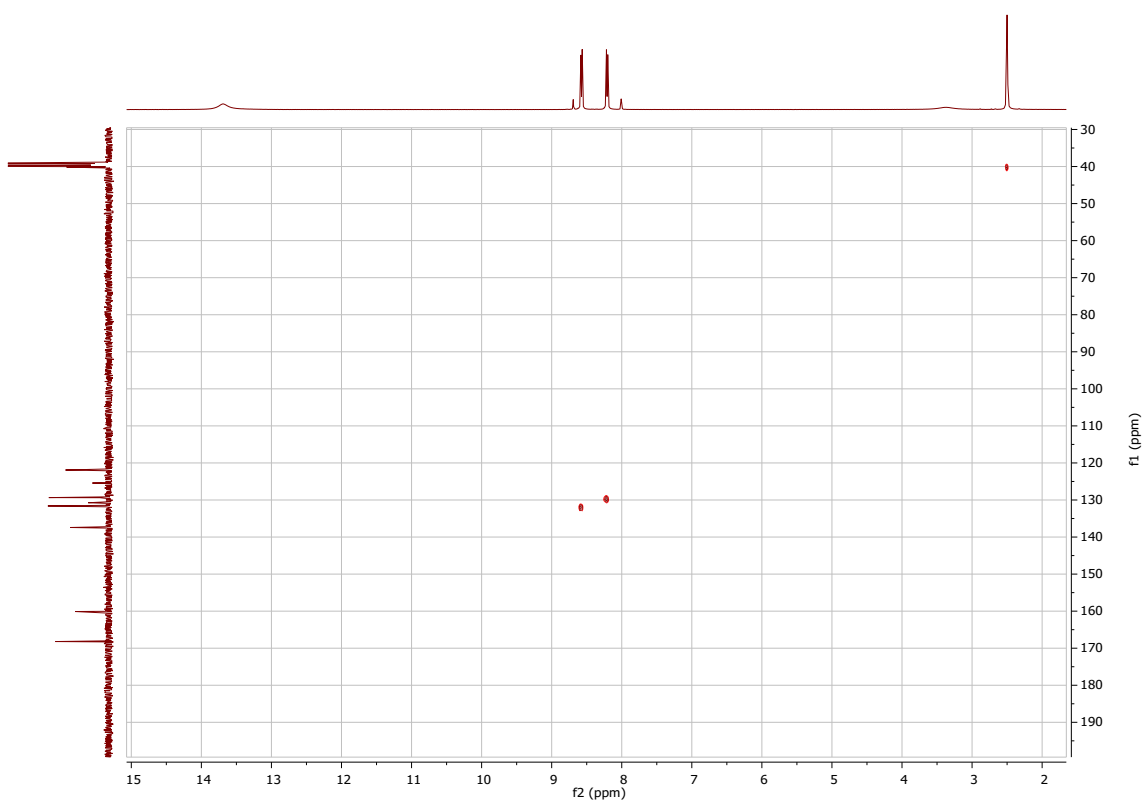**Figure S25.** ^{13}C NMR (101 MHz, DMSO) δ 168.20, 160.10, 137.42, 131.61, 130.74, 129.35, 125.42, 121.91

Figure S26. 2D ^1H and ^{13}C NMR

S7   References

S1   G. M. Sheldrick, SHELXT – Integrated Space-Group and Crystal Structure Determination, *Acta Crystallogr. Sect. A.* 2015, **71**, 3-8.

S2.   G. M. Sheldrick, Crystal Structure Refinement with SHELXL. *Acta Crystallogr. Sect. C.* 2015, **71**, 3-8.

S3   O. V. Dolomanov, L. J. Bourhis, R. J. Gildea, J. A. K. Howard, H. Puschmann, OLEX2: a complete structure solution, refinement and analysis program. *J. Appl. Crystallogr.* 2009, **42**, 339–341.